RSC Advances

PAPER

View Article Online
View Journal | View Issue

Check for updates

Cite this: *RSC Adv.*, 2020, **10**, 38621

Sulfobetaine methacrylate-functionalized graphene oxide-IR780 nanohybrids aimed at improving breast cancer phototherapy†

Miguel M. Leitão,[a] Cátia G. Alves,[a] Duarte de Melo-Diogo,*[a] Rita Lima-Sousa,[a] André F. Moreira [a] and Ilídio J. Correia *[ab]

The application of Graphene Oxide (GO) in cancer photothermal therapy is hindered by its lack of colloidal stability in biologically relevant media and modest Near Infrared (NIR) absorption. In this regard, the colloidal stability of GO has been improved by functionalizing its surface with poly(ethylene glycol) (PEG), which may not be optimal due to the recent reports on PEG immunogenicity. On the other hand, the chemical reduction of GO using hydrazine hydrate has been applied to enhance its photothermal capacity, despite decreasing its cytocompatibility. In this work GO was functionalized with an amphiphilic polymer containing [2-(methacryloyloxy)ethyl]dimethyl-(3-sulfopropyl)ammonium hydroxide (SBMA) brushes and was loaded with IR780, for the first time, aiming to improve its colloidal stability and phototherapeutic capacity. The attained results revealed that the SBMA-functionalized GO displays a suitable size distribution, neutral surface charge and adequate cytocompatibility. Furthermore, the SBMA-functionalized GO exhibited an improved colloidal stability in biologically relevant media, while its non-SBMA functionalized equivalent promptly precipitated under the same conditions. By loading IR780 into the SBMA-functionalized GO, its NIR absorption increased by 2.7-fold, leading to a 1.2 times higher photothermal heating. In *in vitro* cell studies, the combination of SBMA-functionalized GO with NIR light only reduced breast cancer cells' viability to 73%. In stark contrast, by combining IR780 loaded SBMA-functionalized GO and NIR radiation, the cancer cells' viability decreased to 20%, hence confirming the potential of this nanomaterial for cancer photothermal therapy.

Received 1st September 2020
Accepted 14th October 2020

DOI: 10.1039/d0ra07508f

rsc.li/rsc-advances

Open Access Article. Published on 20 October 2020. Downloaded on 12/4/2025 10:06:17 PM.
This article is licensed under a Creative Commons Attribution-NonCommercial 3.0 Unported Licence.

1. Introduction

Photothermal Therapy (PTT) mediated by nanomaterials has been showing promising results in cancer treatment.[1–5] This type of approach explores the ability of photo-responsive nanostructures to passively accumulate at the tumor site (through the Enhanced Permeability and Retention (EPR) effect), and to convert light into heat.[6,7] For this purpose, the use of Near Infrared (NIR; 750–1000 nm) light is essential due to its minimal interactions with biological components (*e.g.* water, melanin, collagen) and high tissue penetration depth, ensuring a spatio-temporal controlled effect.[6,8–10]

Among the different NIR light-responsive nanomaterials, Graphene Oxide (GO) has been receiving great interest for application in cancer therapy.[11–13] Upon interaction with NIR light, GO can produce a temperature increase capable of causing damage to cancer cells.[8,13–15] Furthermore, the aromatic lattice of GO can encapsulate a wide variety of therapeutics, enabling its use in NIR-responsive drug delivery applications.[8,16,17]

Despite its potential, the direct application of GO in cancer PTT is limited by its poor colloidal stability in biologically relevant media.[11,18] As-synthesized GO precipitates in biological fluids, hindering its ability to reach the tumor site.[8,18] This limitation has been solved by functionalizing the surface of GO with poly(ethylene glycol) (PEG) derivatives.[19,20] However, recent reports have disclosed that PEG based coatings can be immunogenic.[21,22] In brief, anti-PEG antibodies are generated at the moment of the first intravenous administration of PEGylated nanomaterials.[23] Then, these anti-PEG antibodies mediate the rapid clearance of the PEG coated nanostructures in subsequent administrations, impairing their tumor homing capacity (known as the accelerated blood clearance phenomenon).[24] These findings highlight the importance of developing novel materials to functionalize GO.

On the other hand, GO presents a modest photothermal capacity, requiring the administration of high dosages or the use of intense radiation to exert an appropriate therapeutic

[a]*CICS-UBI – Centro de Investigação em Ciências da Saúde, Universidade da Beira Interior, 6200-506 Covilhã, Portugal. E-mail: icorreia@ubi.pt; demelodiogo@fcsaude.ubi.pt; Tel: +351 275 329 055*

[b]*CIEPQPF – Departamento de Engenharia Química, Universidade de Coimbra, 3030-790 Coimbra, Portugal*

† Electronic supplementary information (ESI) available. See DOI: 10.1039/d0ra07508f

Open Access Article. Published on 20 October 2020. Downloaded on 12/4/2025 10:06:17 PM.
This article is licensed under a Creative Commons Attribution-NonCommercial 3.0 Unported Licence.

effect.[25–27] To address this problem, GO has been chemically reduced using hydrazine hydrate.[28,29] This chemical process restores the graphitic lattice of this nanomaterial, improving its NIR absorption and hence its photothermal capacity.[28] However, due to the toxicity of hydrazine hydrate, the reduced GO attained using this reducing agent has a weak cytocompatibility even after functionalization.[28,29] Alternatively, other NIR-responsive nanomaterials (*e.g.* gold nanorods, upconversion nanoparticles[30–33]) have been incorporated on the surface of GO to improve its photothermal capacity. Nevertheless, this process is both laborious and complex, limiting the future translation of these hybrid-nanostructures. Therefore, it is also necessary to implement novel approaches to increase the photothermal effect mediated by GO.

In this work, GO was functionalized with an amphiphilic polymer containing [2-(methacryloyloxy)ethyl]dimethyl-(3-sulfopropyl)ammonium hydroxide (SBMA) brushes and was loaded with IR780, for the first time, to improve its colloidal stability and phototherapeutic capacity, respectively. We recently demonstrated that the functionalization of protein based nanoparticles with SBMA can improve their colloidal stability.[7] Furthermore, SBMA brushes are capable of improving nanomaterials' blood circulation time and have not been reported to experience the accelerated blood clearance phenomenon.[34–36] In turn, IR780 (a hydrophobic small molecule) was selected to be loaded on GO due to its good photothermal capacity upon NIR laser irradiation.[7,37–39] Moreover, we recently showed that the optical properties of IR780 are superior to those of other NIR dyes such as Indocyanine Green, IR783, or IR820.[1]

In order to attain the amphiphilic polymer with SBMA brushes, SBMA was grafted into poly(ethyleneimine) (PEI). Then, the resulting polymer was conjugated with hydrolysed poly(maleic anhydride-*alt*-1-octadecene) (PMAO), yielding SBMA-PEI-PMAO (SPP). Subsequently, GO was functionalized with SPP and loaded with IR780 (IR780-SPP/GO) through a simple sonication process. The results revealed that the SPP/GO and IR780-SPP/GO display a neutral surface charge and that maintain their size distribution overtime when in contact with biologically relevant media, demonstrating an improved colloidal stability. In contrast, the non-SBMA functionalized GO (PEI-PMAO coated GO and IR780 loaded PEI-PMAO coated GO) promptly precipitated in the biologically relevant media. By loading IR780 into the SPP/GO, its NIR absorption increased by 2.7-fold, leading to a 1.2 times higher photothermal heating. In *in vitro* cell studies, the combination of SPP/GO with NIR light only reduced breast cancer cells' viability to 73%. In stark contrast, by combining IR780-SPP/GO and NIR radiation, the cancer cells' viability decreased to 20%, hence confirming the IR780-SPP/GO potential for cancer PTT.

2. Materials and methods

2.1. Materials

Michigan Cancer Foundation-7 (MCF-7) cell line and Normal Human Dermal Fibroblasts (NHDF) were obtained from ATCC (Middlesex, UK) and Promocell (Heidelberg, Germany), respectively. 3-(4,5-Dimethylthiazol-2-yl)-5-(3-carboxymethoxyphenyl)-2-(4-sulfophenyl)-2*H*-tetrazolium (MTS) was bought from Promega (Madison, WI, USA). Fetal Bovine Serum (FBS) was acquired from Biochrom AG (Berlin, Germany). 1-Ethyl-3-(3-dimethylaminopropyl)carbodiimide (EDC) was purchased from Merck (Darmstadt, Germany). Dimethyl sulfoxide (DMSO) and methanol were acquired from Fisher Scientific (Oeiras, Portugal). Cell imaging plates were obtained from Ibidi GmbH (Munich, Germany). Cell culture plates and T-flasks were purchased from Thermo Fisher Scientific (Porto, Portugal). GO was obtained from NanoPoz (Umultowska Poznan, Wielkopolska). Branched PEI (M_n 1250 Da), SBMA, Dulbecco's Modified Eagle's Medium-F12 (DMEM-F12), IR780 iodide, *N*-hydroxysuccinimide (NHS), paraformaldehyde, PMAO (average M_n 30 000–50 000 Da) and trypsin were bought from Sigma-Aldrich (Sintra, Portugal). Calcein-AM, Hoechst 33342® and Propidium Iodide (PI) were obtained from Thermo Fisher Scientific (Porto, Portugal). Water used in all experiments was double deionized (0.22 μm filtered, 18.2 MΩ cm).

2.2. Methods

2.2.1. Synthesis and characterization of SPP. The synthesis of SPP was a tri-step process. Initially, SBMA was covalently attached to PEI, through a Michael addition, following the method described by Venault *et al.* with slight modifications.[40] In brief, SBMA (1.176 g) and PEI (0.5 g) dissolved in 5 mL of water were reacted under reflux for 6 h at 90 °C. Then, the solution was dialysed against water (500–1000 Da molecular weight cut-off membrane) for 2 days and freeze-dried (ScanVac CoolSafe, LaboGene ApS, Lynge, Denmark), yielding SBMA-PEI (SP).

Subsequently, the hydrolysis of PMAO maleic anhydride rings was performed as we have previously described.[37] Briefly, an aqueous solution (4 mL) containing PMAO (0.2 g) and NaOH (2 N) was stirred for 5 h at room temperature. Then, the solution's pH was adjusted to 7 using HCl, followed by dialysis against water for 1 day (14 000 Da molecular weight cut-off membrane). The recovered solution was freeze-dried, yielding hydrolysed PMAO.

Finally, to produce SPP, SP was attached to the hydrolysed PMAO carboxyl groups using the carbodiimide chemistry.[29] First, hydrolysed PMAO (50 mg) was activated with EDC (6 mg) and NHS (3 mg) in 25 mL of DMSO. Subsequently, 50 mg of SP in water (25 mL) was added to the above solution. After reacting for 6 h at room temperature, the solution was dialysed against water for 3 days (14 000 Da molecular weight cut-off membrane) and freeze-dried, yielding SPP.

As a control, PEI-PMAO (PP) was also produced as described above using hydrolysed PMAO (50 mg), PEI (50 mg), EDC (6 mg) and NHS (3 mg).

The successful synthesis of hydrolysed PMAO, SP, SPP and PP was confirmed by Fourier Transform Infrared Spectroscopy (FTIR) using a Nicolet iS10 spectrometer (Thermo Scientific Inc., MA, USA) with a spectral width ranging from 4000 to 600 cm^{-1}. Moreover, proton nuclear magnetic resonance (^1H NMR) spectra of SBMA, PEI, SP, hydrolysed PMAO and SPP were acquired by using a Brüker Avance III 400 MHz spectrometer

 This journal is © The Royal Society of Chemistry 2020

Open Access Article. Published on 20 October 2020. Downloaded on 12/4/2025 10:06:17 PM.
This article is licensed under a Creative Commons Attribution-NonCommercial 3.0 Unported Licence.

(Brüker Scientific Inc., NY, USA). For the ^{1}H NMR experiments, SBMA, PEI and SP (in 9 : 1 (v/v) H_2O/D_2O), SPP (in 1 : 1 (v/v) DMSO-d_6/(9 : 1 (v/v) H_2O/D_2O)) and hydrolysed PMAO (in DMSO-d_6) were analysed at 298 K. MNova software (Mestrelab Research, SL, Santiago de Compostela, Spain) was used to process and analyse the acquired spectra.

2.2.2. Assembly of IR780-SPP/GO. The assembly of IR780-SPP/GO was performed using a simple sonication approach as we have previously described.[8] Initially, an aqueous solution containing GO (100 μg mL^{-1}; 1 mL) and SPP (500 μg) was sonicated for 60 min (Branson 5800, Branson Ultrasonics, CT, USA). Then, IR780 (5 μg; dissolved in methanol) was added to the SPP-GO solution, followed by 30 min of sonication. Afterwards, this solution was dialysed (500–1000 Da molecular weight cut-off membrane) against water for 90 min and centrifuged to remove non-loaded IR780 and/or any aggregates, yielding IR780-SPP/GO. To produce IR780 loaded PEI-PMAO coated GO (IR780-PP/GO), the methodology was the same as described above but using PP instead of SPP. Non-loaded SPP/GO and non-loaded PEI-PMAO coated GO (PP/GO) were produced as described above without the IR780 addition step.

2.2.3. Characterization of nanomaterials' physicochemical and photothermal properties. FTIR, UV-vis-NIR absorption spectroscopy (Evolution 201 spectrophotometer, Thermo Fisher Scientific Inc., Massachusetts, USA), and Energy-Dispersive X-ray Spectroscopy (EDS; Bruker, Karlsruhe, Germany) analysis were performed to confirm the functionalization of GO with SPP. The size distribution (in water) and zeta potential (in DMEM-F12 medium supplemented with FBS) of SPP/GO and IR780-SPP/GO were determined on a Zetasizer Nano ZS (Malvern Instruments Ltd., Worcestershire, UK). Furthermore, the colloidal stability of SPP/GO, IR780-SPP/GO, PP/GO and IR780-PP/GO was also evaluated in water and cell culture medium (DMEM-F12 supplemented with 10% (v/v) of FBS). Transmission Electron Microscopy (TEM) was also used to confirm the lateral dimensions of SPP/GO, by using an HT7700 microscope (Hitachi, Japan) operated at an accelerating voltage of 100 kV (samples were stained with phosphotungstic acid (2% (w/v))).

To verify SPP/GO and IR780-SPP/GO ability to interact with NIR light, the samples' absorbance was evaluated by UV-vis-NIR absorption spectroscopy. In turn, the photothermal capacity of SPP/GO and IR780-SPP/GO was determined by measuring the temperature variations induced by these nanoformulations (at different GO concentrations) over a period of 8 min of NIR irradiation (808 nm, 1.7 W cm^{-2}) with a thermocouple thermometer.[37] Water was used as a control.

Finally, the content of IR780 in SPP/GO was determined by absorption spectroscopy. For such, IR780-SPP/GO was resuspended in a water/methanol solution (1 : 1 (v/v)) and the samples' absorbance at 808 and 890 nm were analysed. First, the concentration of GO in IR780-SPP/GO was determined by using a standard curve of GO at 890 nm (IR780 and SPP do not absorb at this wavelength). Then, the determined concentration of GO and a standard curve of GO at 808 nm were used to find the absorption of GO at this wavelength. Subsequently, the absorption of GO at 808 nm was subtracted to that of IR780-SPP/GO at 808 nm, yielding the absorption of IR780 at 808 nm (SPP does not absorb at this wavelength). Finally, the absorption of IR780 at 808 nm and a standard curve of IR780 at this wavelength were used to determine IR780 concentration. Then, the encapsulation efficiency of IR780 was determined as described in ref. 37.

2.2.4. Evaluation of the cytocompatibility of SPP/GO. The cytocompatibility of SPP/GO towards MCF-7 cells (breast cancer cell model) and NHDF (normal cell model) was characterized using the MTS method as previously described by our group.[41] Cells were cultured in DMEM-F12 medium supplemented with 10% (v/v) FBS and 1% (v/v) streptomycin/gentamicin in a humidified incubator (37 °C, 5% CO_2). Briefly, cells were seeded at a density of 1×10^4 cells per well in 96-well plates. After 24 h, the medium was replaced by fresh culture medium containing different concentrations of SPP/GO (1–50 μg mL^{-1} of GO equivalents). After 24 and 48 h, the medium was removed and cells were incubated with 120 μL of fresh medium containing MTS (20 μL) for 4 h (37 °C, 5% CO_2). Then, cells' viability was determined by analysing the samples' absorbance at 490 nm using a microplate reader (Bio-Rad xMark microplate spectrophotometer). Non treated cells were used as the negative control (K^-) while cells treated with ethanol 70% were used as the positive control (K^+).

2.2.5. *In vitro* evaluation of the phototherapeutic effect mediated by SPP/GO and IR780-SPP/GO. The photothermal effect mediated by SPP/GO and IR780-SPP/GO was evaluated as previously described by us.[11] Briefly, MCF-7 cells were seeded at a density of 1×10^4 cells per well in 96-well plates. After 24 h, the medium was removed, and the cells were incubated with fresh medium containing different concentrations of SPP/GO (at 30 and 50 μg mL^{-1} of GO equivalents) or IR780-SPP/GO (at 30/1.44 and 50/2.40 μg mL^{-1} of GO/IR780 equivalents). After 4 h of incubation, cells were irradiated with NIR light (808 nm, 1.7 W cm^{-2}, 8 min). After 24 h incubation, cells' viability was determined using the MTS method as described in Section 2.2.4.

To visualize the different phototherapeutic effects, MCF-7 cells incubated with SPP/GO (at 50 μg mL^{-1} of GO equivalents) or IR780-SPP/GO (at 50/2.40 μg mL^{-1} of GO/IR780 equivalents) and exposed to NIR light (as described above), were stained with Calcein-AM/PI (according to the manufacture's protocol) and were imaged by Confocal Laser Scanning Microscopy (CLSM) using a Zeiss LSM 710 confocal microscope (Carl Zeiss AG, Oberkochen, Germany).[37] To analyse the uptake of IR780-SPP/GO by MCF-7 cells, these were incubated during 4 h with this nanomaterial. Afterwards, CLSM images were acquired by taking advantage from the IR780 intrinsic fluorescence.[37]

2.2.6. Statistical analysis. To compare multiple groups, one-way Analysis of Variance (ANOVA) was used with the Student–Newman–Keuls test. A value of p lower than 0.05 ($p < 0.05$) was considered statistically significant. Data analysis was performed in GraphPad Prism v6.0 (Trial version, GraphPad Software, CA, USA).

Open Access Article. Published on 20 October 2020. Downloaded on 12/4/2025 10:06:17 PM.
This article is licensed under a Creative Commons Attribution-NonCommercial 3.0 Unported Licence.

3. Results and discussion

3.1. Formulation and characterization of SPP/GO and IR780-SPP/GO

In order to improve the colloidal stability of GO, this nanomaterial was functionalized with a SBMA-based amphiphilic polymer (SPP). Then, the SPP-functionalized GO was loaded with IR780 with the intent to improve its photothermal capacity – Fig. 1(A). The successful synthesis of SPP was confirmed by FTIR and ^{1}H NMR (data presented in the ESI – Fig. S2, S3, S5 and S6†).

SPP was used to functionalize GO through a simple sonication process, yielding SPP/GO. In this process, the alkyl chain of SPP adsorbs on the aromatic matrix of GO by taking advantage from hydrophobic–hydrophobic interactions. The functionalization of GO with SPP was confirmed by FTIR, which revealed that the spectrum of SPP/GO displays the S=O stretch peak characteristic of SPP (Fig. S7†). When compared to GO, the absorption spectrum of SPP/GO presented an augmented absorption in the 200–290 nm range (Fig. S8†). The analysis of SPP demonstrated that this SBMA-based amphiphilic polymer also presents a strong absorption between 200 and 290 nm (Fig. S8†). In this way, the increased absorption of SPP/GO in this range is also indicative of the functionalization of GO with SPP. The EDS analysis revealed that SPP/GO has a carbon : oxygen : sulfur ratio of about 53 : 46 : 1, which also supports the presence of SPP in SPP/GO (the carbon : oxygen ratio of GO was determined to be 66 : 34 being in agreement with literature reports[8,42]). Moreover, the Dynamic Light Scattering (DLS) analysis indicated that GO maintained its nanometric size distribution upon functionalization with SPP (Fig. 1(B)). The lateral dimensions of SPP/GO were then confirmed by TEM (Fig. S9†), revealing that this nanomaterial has a size compatible with its application in cancer therapy.[6,8]

Then, IR780 was loaded in SPP/GO by taking advantage from hydrophobic interactions and π–π stacking. Both SPP/GO and IR780-SPP/GO demonstrated a similar size distribution, indicating that the IR780 loading did not affect the nanomaterials' size (Fig. 1(B)). The IR780 encapsulation efficiency in IR780-SPP/GO was of about 74 ± 1%. Moreover, the water solubility of IR780 after being encapsulated in SPP/GO was 3.69 μg mL^{-1}. Considering that the water solubility of free IR780 is about 0.40 μg mL^{-1},[43] the IR780 loading into SPP/GO led to a 9.23-fold increase in its solubility. Furthermore, the IR780-SPP/GO adsorbed 0.048 ± 0.004 μg of IR780 per μg of GO, which is in line with the drug loading capacity of GO derivatives (please note that non-loaded GO is removed during the centrifugation step, leading to a higher drug loading capacity).[11]

The zeta potential of SPP/GO (−7.7 ± 0.4 mV) and IR780-SPP/GO (−8.1 ± 0.7 mV) revealed that these formulations have a neutral surface charge (nanomaterials with a zeta potential between −10 and +10 mV are considered to display a neutral

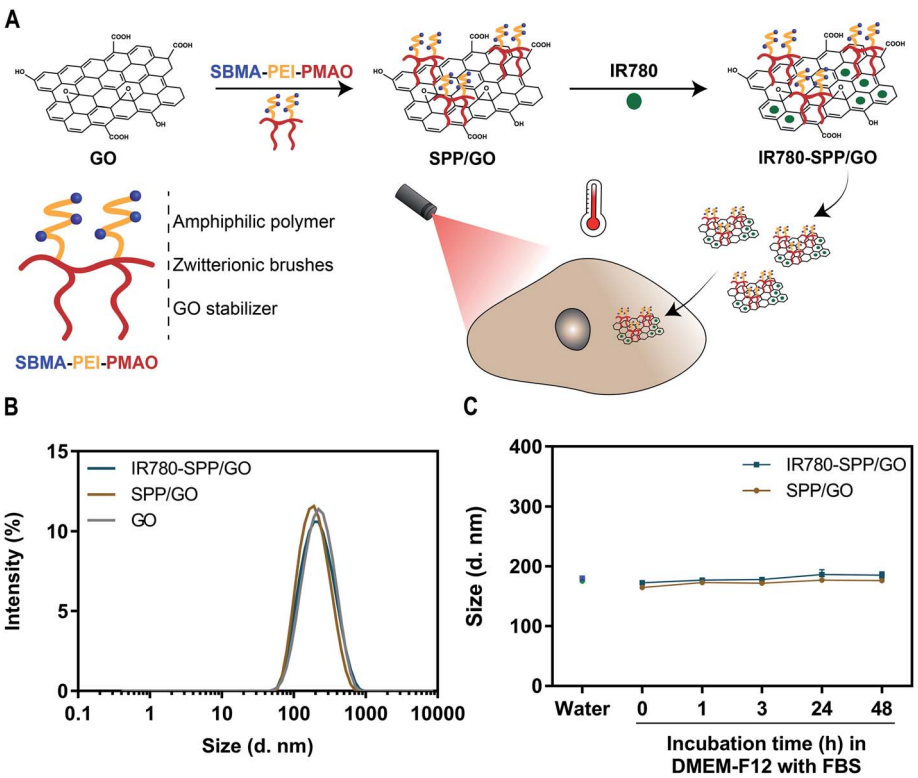

Fig. 1 Preparation and characterization of SPP/GO and IR780-SPP/GO. Schematic representation of SPP/GO and IR780-SPP/GO assembly and application in cancer therapy (A). DLS size distribution of GO, SPP/GO and IR780-SPP/GO (B). Size of SPP/GO and IR780-SPP/GO in water and in DMEM-F12 medium (supplemented with 10% (v/v) of FBS) at different time points (C). Each bar represents the mean ± Standard Deviation (S.D.) (n = 3).

 This journal is © The Royal Society of Chemistry 2020

Open Access Article. Published on 20 October 2020. Downloaded on 12/4/2025 10:06:17 PM.
This article is licensed under a Creative Commons Attribution-NonCommercial 3.0 Unported Licence.

surface charge[44,45]). Taking into account that the zeta potential of GO was determined to be -10.4 ± 0.6 mV, this data indicates that the SPP coating can induce the neutralization of the surface charge of these nanomaterials. In fact, several nanomaterials functionalized with SBMA brushes also revealed a neutral surface charge.[7,36,46] As importantly, neutrally charged nanomaterials (zeta potential between −10 and +10 mV) are considered in the literature as optimal due to their improved blood circulation time, which favours their tumor uptake.[6]

Lastly, the colloidal stability of SPP/GO and IR780-SPP/GO overtime in water and in cell culture medium (DMEM-F12 supplemented with 10% (v/v) of FBS) was investigated (Fig. S10†). Both SPP/GO and IR780-SPP/GO maintained their size distribution overtime (Fig. 1(C)). As a control, the stability of PP/GO and IR780-PP/GO was also analysed, being verified that these non-SBMA grafted nanomaterials promptly precipitate in water and in culture medium (Fig. S11†). In this way, the presence of the SBMA in the SPP/GO and IR780-SPP/GO endows these nanomaterials an excellent colloidal stability. In fact, the SBMA functionalization can reduce the adsorption of proteins on nanomaterials' surface, enhancing their stability during circulation and possibility favouring their tumor uptake.[36] Together, this data indicates that the SPP/GO and IR780-SPP/GO have suitable physicochemical properties for application in cancer therapy.

3.2. Phototherapeutic capacity of SPP/GO and IR780-SPP/GO

To analyse the ability of SPP/GO and IR780-SPP/GO to interact with the NIR radiation, their absorption spectra was acquired (Fig. 2(A)). As expected, SPP/GO demonstrated a broad absorption in the NIR region (750–1000 nm), which is a characteristic feature of GO derivatives.[11,29] In turn, the absorption spectrum of IR780-SPP/GO (Fig. 2(A)) displayed the GO characteristic absorption band as well as an increased absorption in the 680–870 nm range due to the presence of IR780 in this nanomaterial (Fig. 2(A) and (B)). Compared to SPP/GO, the IR780-SPP/GO presented a 2.7-fold higher absorption at 808 nm. Since 808 nm light will be used in the photothermal experiments, the enhanced absorption of IR780-SPP/GO at this wavelength may produce a better therapeutic outcome.

Then, the photothermal capacity of SPP/GO and IR780-SPP/GO was investigated by exposing these nanomaterials to NIR light (808 nm, 1.7 W cm^{-2}, 8 min) and recording the temperature changes (Fig. 2(C) and (D)). At the maximum concentration tested (50 μg mL^{-1} of GO equivalents), the SPP/GO could produce a temperature increase to about 14.9 °C after 8 min of irradiation (Fig. 2(C)). Such temperature variation is sufficiently high to cause damage to cancer cells.[6,47] At the same concentration, the IR780-SPP/GO generated a temperature increase to 13.3 °C just after 2 min of irradiation (Fig. 2(D)). After 8 min of laser exposure, the IR780-SPP/GO produced a photoinduced heat to 18.4 °C (Fig. 2(D)). In this way, the incorporation of IR780 in GO derivatives can be pursued to improve their photothermal potential. Moreover, it was found that the NIR radiation does not increase meaningfully the water temperature (ΔT < 3.6 °C). Such result is explained by the minimal interactions of the NIR radiation with water, thus suggesting that SPP/GO and

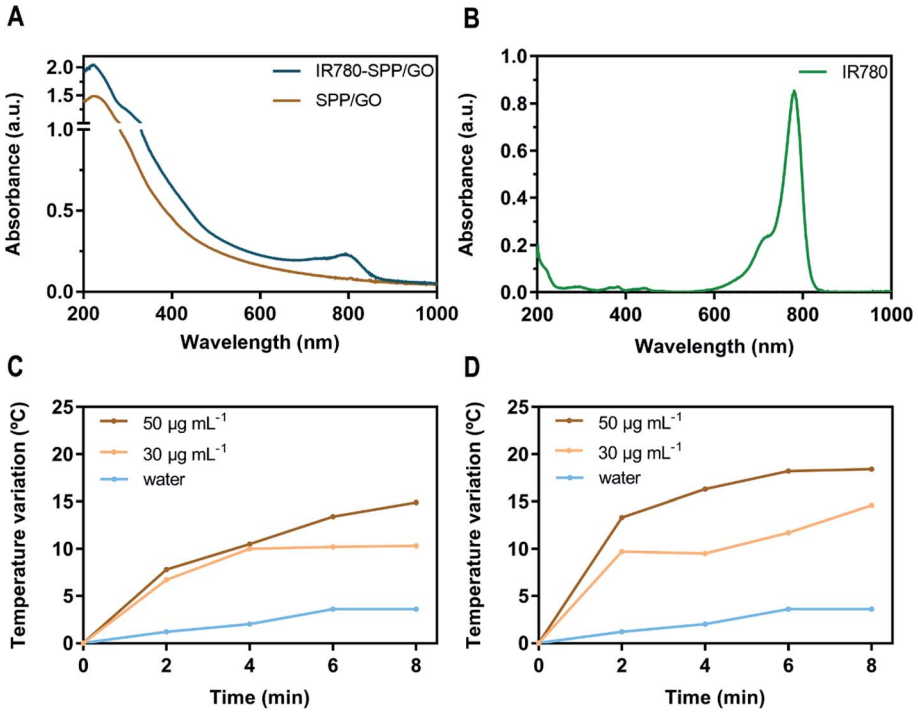

Fig. 2 Optical and photothermal properties of SPP/GO and IR780-SPP/GO. Absorption spectra of SPP/GO and IR780-SPP/GO (20 μg mL^{-1} of GO equivalents; in water) (A). Absorption spectrum of free IR780 (2.5 μg mL^{-1} in methanol) (B). Temperature variation curves of SPP/GO (C) and of IR780-SPP/GO (D) at different concentrations (of GO equivalents) during 8 min of NIR irradiation (808 nm, 1.7 W cm^{-2}).

Open Access Article. Published on 20 October 2020. Downloaded on 12/4/2025 10:06:17 PM.
This article is licensed under a Creative Commons Attribution-NonCommercial 3.0 Unported Licence.

IR780-SPP/GO can produce a spatio-temporal controlled photothermal heating.

For instance, Ma *et al.* prepared gold clusters grafted into reduced GO (prepared using hydrazine hydrate),[48] that could generate a temperature increase of about 13.7 °C after 5 min of irradiation (808 nm, 2.2 W cm^{-2}) at a concentration of 90 μg mL^{-1} (of nanohybrids). Herein, the IR780-SPP/GO produced a photoinduced heat of 18.2 °C after 6 min of irradiation (808 nm, 1.7 W cm^{-2}) using only 50 μg mL^{-1} of GO. In this way, the incorporation of IR780 in GO is a promising alternative to using hydrazine hydrate for improving the GO photothermal capacity. Together, these results confirm the photothermal potential of IR780-SPP/GO.

3.3. Cytocompatibility of SPP/GO

Before determining the phototherapeutic potential of SPP/GO, its cytocompatibility when non-irradiated with NIR light was determined (Fig. 3). For such, MCF-7 cells and NHDF were used as models of breast cancer cells and healthy cells, respectively. Both MCF-7 cells (Fig. 3(A)) and NHDF (Fig. 3(B)) incubated with SPP/GO (up to 50 μg mL^{-1} of GO equivalents) did not suffer meaningful alterations on their viability, even after 24 and 48 h of incubation (cell viability > 86%).

Some studies have reported that nanomaterials functionalized only with PEI can be cytotoxic due to the highly positive surface charge of this polymer.[49–51] For instance, Kievit *et al.* showed that PEI coated nanoparticles (zeta potential ≈ +37 mV) are highly cytotoxic (cell viability reduced to about 10%).[49] Herein, even though SPP contains PEI in its composition, the surface charge neutralization mediated by the SBMA grafting may have played a critical role in rendering SPP/GO cytocompatible. In fact, this data is also in line with the excellent biocompatibility of SBMA-functionalized nanomaterials.[7,52,53]

3.4. Phototherapeutic effect mediated by SPP/GO and IR780-SPP/GO

Finally, the phototherapeutic effect mediated by SPP/GO and IR780-SPP/GO towards MCF-7 cells was investigated (Fig. 4(A)).

As expected, non-irradiated SPP/GO and IR780-SPP/GO did not induce cytotoxicity towards MCF-7 cells (Fig. 4(B)). Such is in agreement with the cytocompatible profile of SPP/GO and with the fact that non-irradiated IR780-based nanomaterials are generally non-cytotoxic.[7,37,54]

At the highest concentration tested (50 μg mL^{-1} of GO equivalents), the combination of SPP/GO with NIR light (808 nm, 1.7 W cm^{-2}, 8 min) only caused a reduction of breast cancer cells' viability to 73% (Fig. 4(B)). In stark contrast, the photothermal effect mediated by IR780-SPP/GO induced a reduction in the viability of cancer cells to about 20% (Fig. 4(B)). Therefore, by incorporating IR780 in the SPP/GO, its phototherapeutic capacity was increased by 3.65-times (Fig. 4(B)). The enhanced therapeutic capacity of IR780-SPP/GO is related with its higher photothermal capacity when compared to that of SPP/GO (Fig. 2(C) and (D)). As importantly, cancer cells treated with only NIR light did not suffer any meaningful alteration in their viability, which is in agreement with the weak/minimal interactions of this radiation with biological components.

To further confirm these results, the Calcein-AM (labels live cells) and PI (labels dead cells) staining of MCF-7 cells after the different treatments was performed (Fig. 4(C) and (D)). In agreement with the cell viability results, the CLSM images of cells exposed to SPP/GO, SPP/GO plus NIR light, and IR780-SPP/GO revealed that these were broadly stained with Calcein-AM (Fig. 4(C) and (D)). Accordingly, cells exposed to SPP/GO plus NIR light were stained with both Calcein-AM and PI (Fig. 4(D)). Furthermore, a very high number of PI stained cells was imaged on the IR780-SPP/GO plus NIR light group (Fig. 4(D)). The ability of IR780-SPP/GO to become internalized by MCF-7 cells was also confirmed by CLSM by taking advantage from the IR780 intrinsic fluorescence (Fig. S12†). Together, these results suggest that IR780-SPP/GO may produce an on-demand therapeutic effect upon NIR laser irradiation.

For instance, PEGylated polypyrrole-GO-gold nanohybrids, when administered at 60 μg mL^{-1}, could reduce the viability of cancer cells to 48% upon NIR laser irradiation (808 nm, 1.75 W cm^{-2}, 10 min).[55] In another work, the photothermal effect mediated by PEGylated GO/CuS hybrids induced a reduction of

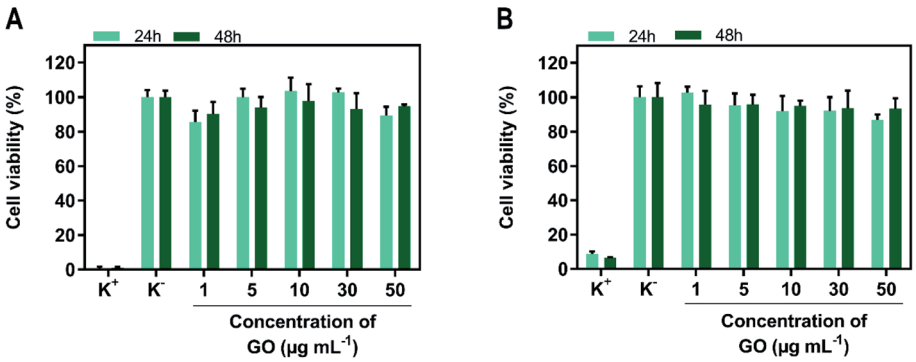

Fig. 3 Evaluation of the cytocompatibility of SPP/GO. Cell viability of MCF-7 cells (A) and NHDF (B) incubated with SPP/GO, at different concentrations of GO, during 24 and 48 h. K^- represents the negative control and K^+ the positive control. Each bar represents the mean ± S.D. (n = 5).

 This journal is © The Royal Society of Chemistry 2020

Open Access Article. Published on 20 October 2020. Downloaded on 12/4/2025 10:06:17 PM.
This article is licensed under a Creative Commons Attribution-NonCommercial 3.0 Unported Licence.

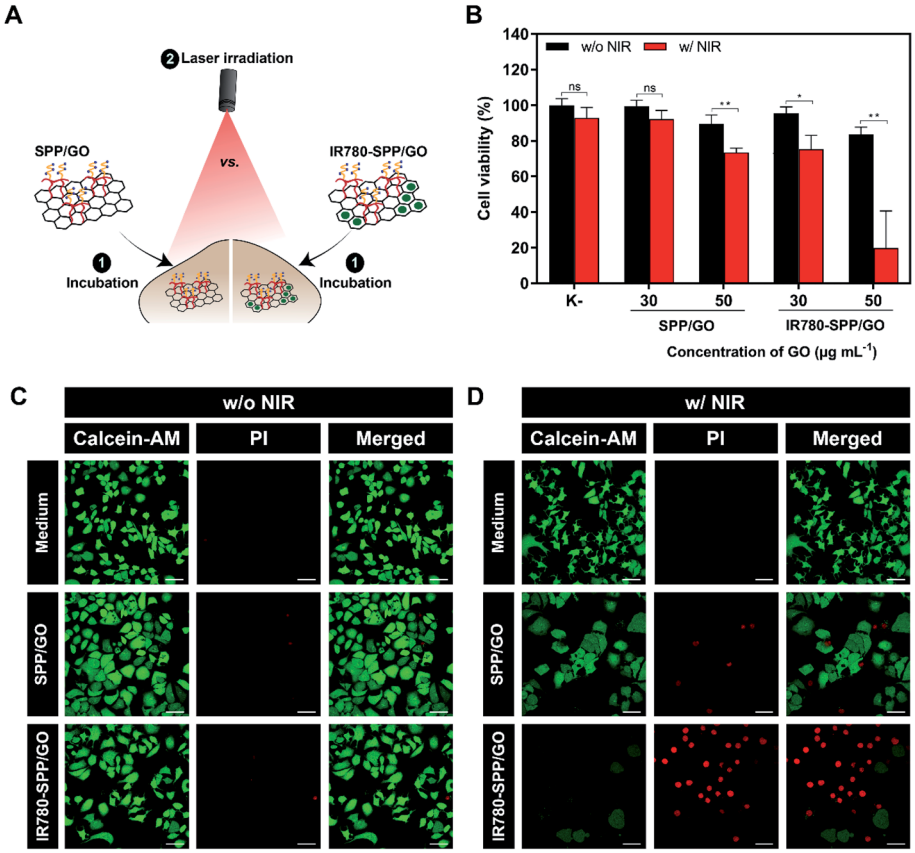

Fig. 4 Determination of the therapeutic capacity of SPP/GO and IR780-SPP/GO. Schematic representation of the procedure used to evaluate the phototherapeutic effect of SPP/GO or IR780-SPP/GO towards MCF-7 cells (A). Therapeutic effect mediated by SPP/GO and IR780-SPP/GO towards MCF-7 cells without (w/o NIR) and with NIR (w/NIR) laser irradiation (808 nm, 1.7 W cm $^{-2}$, 8 min) (B). K^- w/o NIR represents the negative control, while K^- w/NIR represents cells solely exposed to NIR light. Data represents mean ± S.D., $n = 5$, (*$p < 0.01$, **$p < 0.0001$), ns = non-significant. CLSM images of MCF-7 cells stained with Calcein-AM/PI after exposure to SPP/GO or IR780-SPP/GO w/o NIR (C) or w/NIR laser irradiation (808 nm, 1.7 W cm $^{-2}$, 8 min) (D). Medium w/o NIR represents the control for live cells, while medium w/NIR represents cells solely exposed to NIR light. Green channel: Calcein-AM; red channel: PI. Scale bars correspond to 50 μm.

cancer cells' viability to 44% at a concentration of 500 μg mL^{-1} of nanohybrids (980 nm, 1 W cm^{-2}, 10 min).[33] In this study, the photothermal effect mediated by IR780-SPP/GO led to a decrease on cancer cells' viability to 20%, using a low dose of photothermal agents (50/2.40 μg mL $^{-1}$ of GO/IR780 equivalents) and a shorter irradiation time (808 nm, 1.7 W cm^{-2}, 8 min). In this way, IR780-SPP/GO are promising nanomaterials for the PTT of breast cancer cells.

4. Conclusion

In this work, GO was functionalized with an amphiphilic polymer containing SBMA brushes and was loaded with IR780, for the first time, with the intent to improve its colloidal stability and phototherapeutic capacity. The results revealed that the SPP/GO and IR780-SPP/GO display a neutral surface charge and that maintain their size distribution overtime when in contact with biologically relevant media, demonstrating an improved colloidal stability. In contrast, the non-SBMA functionalized GO (PP/GO and IR780-PP/GO) promptly precipitated in this media. By loading IR780 into the SPP/GO, its NIR absorption increased by 2.7-fold, leading to a 1.2-times higher photothermal heating. In *in vitro* cell studies, the combination of SPP/GO with NIR light only reduced breast cancer cells' viability to 73%. In stark contrast, by combining IR780-SPP/GO and NIR radiation, the cancer cells' viability decreased to 20%, hence confirming the IR780-SPP/GO phototherapeutic potential. Overall, the IR780-SPP/GO presents an improved colloidal stability and enhanced photothermal capacity, rendering it a great potential for future application in cancer PTT.

Abbreviation list

ANOVA	Analysis of variance
CLSM	Confocal laser scanning microscopy
DLS	Dynamic light scattering
DMEM-F12	Dulbecco's modified eagle's medium-F12
DMSO	Dimethyl sulfoxide
EDC	1-Ethyl-3-(3-dimethylaminopropyl)carbodiimide
EDS	Energy-dispersive X-ray spectroscopy
EPR	Enhanced permeability and retention
FBS	Fetal bovine serum

Open Access Article. Published on 20 October 2020. Downloaded on 12/4/2025 10:06:17 PM.
This article is licensed under a Creative Commons Attribution-NonCommercial 3.0 Unported Licence.

FTIR	Fourier transform infrared spectroscopy
GO	Graphene oxide
^{1}H NMR	Proton nuclear magnetic resonance
IR780-PP/GO	IR780 loaded PEI-PMAO functionalized GO
IR780-SPP/GO	IR780 loaded SBMA-PEI-PMAO functionalized GO
MCF-7	Michigan cancer foundation-7
MTS	3-(4,5-Dimethylthiazol-2-yl)-5-(3-carboxymethoxyphenyl)-2-(4-sulfophenyl)-2*H*-tetrazolium
NHDF	Normal human dermal fibroblasts
NHS	*N*-Hydroxysuccinimide
NIR	Near infrared
Ns	Non-significant
PEG	Poly(ethylene glycol)
PEI	Poly(ethyleneimine)
PI	Propidium iodide
PMAO	Poly(maleic anhydride-*alt*-1-octadecene)
PP	PEI-PMAO
PP/GO	PEI-PMAO functionalized GO
PTT	Photothermal therapy
SBMA	[2-(Methacryloyloxy)ethyl]dimethyl-(3-sulfopropyl) ammonium hydroxide
S.D.	Standard deviation
SP	SBMA-PEI
SPP	SBMA-PEI-PMAO
SPP/GO	SBMA-PEI-PMAO functionalized GO
TEM	Transmission electron microscopy

Conflicts of interest

There are no conflicts to declare.

Acknowledgements

This work was supported by FEDER (ERDF) funds through the POCI – COMPETE 2020 – Operational Programme Competitiveness and Internationalisation in Axis I – Strengthening Research, Technological Development and Innovation (Project POCI-01-0145-FEDER-007491) and National Funds by FCT (Portugal) – Foundation for Science and Technology (Project UID/Multi/00709/2013). The funding from CENTRO-01-0145-FEDER-028989 and POCI-01-0145-FEDER-031462 is also acknowledged. Duarte de Melo-Diogo acknowledges CENTRO-01-0145-FEDER-028989 for the funding given on the form of a research contract. Cátia G. Alves and Rita Lima-Sousa acknowledge individual PhD fellowships from FCT (SFRH/BD/145386/2019 and SFRH/BD/144922/2019).

References

1 M. M. Leitão, D. de Melo-Diogo, C. G. Alves, R. Lima-Sousa and I. J. Correia, Prototypic heptamethine cyanine incorporating nanomaterials for cancer phototheragnostic, *Adv. Healthcare Mater.*, 2020, **9**(6), 1901665.

2 X. Fu, H. Bai, F. Lyu, L. Liu and S. Wang, Conjugated polymer nanomaterials for phototherapy of cancer, *Chem. Res. Chin. Univ.*, 2020, **36**(2), 237–242.

3 B. P. Jiang, B. Zhou, Z. Lin, H. Liang and X. C. Shen, Recent advances in carbon nanomaterials for cancer phototherapy, *Chem.–Eur. J.*, 2019, **25**(16), 3993–4004.

4 J. B. Vines, J.-H. Yoon, N.-E. Ryu, D.-J. Lim and H. Park, Gold nanoparticles for photothermal cancer therapy, *Front. Chem.*, 2019, **7**, 167.

5 V. Agarwal, N. Varghese, S. Dasgupta, A. Sood and K. Chatterjee, Engineering a 3D MoS2 foam using keratin exfoliated nanosheets, *Chem. Eng. J.*, 2019, **374**, 254–262.

6 D. de Melo-Diogo, C. Pais-Silva, D. R. Dias, A. F. Moreira and I. J. Correia, Strategies to improve cancer photothermal therapy mediated by nanomaterials, *Adv. Healthcare Mater.*, 2017, **6**(10), 1700073.

7 C. G. Alves, D. de Melo-Diogo, R. Lima-Sousa and I. J. Correia, IR780 loaded sulfobetaine methacrylate-functionalized albumin nanoparticles aimed for enhanced breast cancer phototherapy, *Int. J. Pharm.*, 2020, **582**, 119346.

8 D. de Melo-Diogo, C. Pais-Silva, E. C. Costa, R. O. Louro and I. J. Correia, D-α-tocopheryl polyethylene glycol 1000 succinate functionalized nanographene oxide for cancer therapy, *Nanomedicine*, 2017, **12**(5), 443–456.

9 V. Agarwal and K. Chatterjee, Recent advances in the field of transition metal dichalcogenides for biomedical applications, *Nanoscale*, 2018, **10**(35), 16365–16397.

10 Y. Xuan, R.-Y. Zhang, D.-H. Zhao, X.-S. Zhang, J. An, K. Cheng, *et al.*, Ultrafast synthesis of gold nanosphere cluster coated by graphene quantum dot for active targeting PA/CT imaging and near-infrared laser/pH-triggered chemo-photothermal synergistic tumor therapy, *Chem. Eng. J.*, 2019, **369**, 87–99.

11 D. de Melo-Diogo, E. C. Costa, C. G. Alves, R. Lima-Sousa, P. Ferreira, R. O. Louro, *et al.*, POxylated graphene oxide nanomaterials for combination chemo-phototherapy of breast cancer cells, *Eur. J. Pharm. Biopharm.*, 2018, **131**, 162–169.

12 M. Zhang, F. Wu, W. Wang, J. Shen, N. Zhou and C. Wu, Multifunctional nanocomposites for targeted, photothermal, and chemotherapy, *Chem. Mater.*, 2018, **31**(6), 1847–1859.

13 D. de Melo-Diogo, R. Lima-Sousa, C. G. Alves and I. J. Correia, Graphene family nanomaterials for application in cancer combination photothermal therapy, *Biomater. Sci.*, 2019, **7**(9), 3534–3551.

14 D. de Melo-Diogo, R. Lima-Sousa, C. G. Alves, E. C. Costa, R. O. Louro and I. J. Correia, Functionalization of graphene family nanomaterials for application in cancer therapy, *Colloids Surf., B*, 2018, **171**, 260–275.

15 L. Yi, Y. Zhang, X. Shi, X. Du, X. Wang, A. Yu, *et al.*, Recent progress of functionalised graphene oxide in cancer therapy, *J. Drug Targeting*, 2019, **27**(2), 125–144.

16 H. Zhu, J. Deng, Y. Yang, Y. Li, J. Shi, J. Zhao, *et al.*, Cobalt nanowire-based multifunctional platform for targeted chemo-photothermal synergistic cancer therapy, *Colloids Surf., B*, 2019, **180**, 401–410.

 This journal is © The Royal Society of Chemistry 2020

Open Access Article. Published on 20 October 2020. Downloaded on 12/4/2025 10:06:17 PM. This article is licensed under a Creative Commons Attribution-NonCommercial 3.0 Unported Licence.

17 G. Chauhan, V. Chopra, A. Tyagi, G. Rath, R. K. Sharma and A. K. Goyal, "Gold nanoparticles composite-folic acid conjugated graphene oxide nanohybrids" for targeted chemo-thermal cancer ablation: in vitro screening and in vivo studies, *Eur. J. Pharm. Sci.*, 2017, **96**, 351–361.

18 Z. Liu, J. T. Robinson, X. Sun and H. Dai, PEGylated nanographene oxide for delivery of water-insoluble cancer drugs, *J. Am. Chem. Soc.*, 2008, **130**(33), 10876–10877.

19 S. Parveen and S. K. Sahoo, Long circulating chitosan/PEG blended PLGA nanoparticle for tumor drug delivery, *Eur. J. Pharmacol.*, 2011, **670**(2–3), 372–383.

20 J. C. Y. Kah, K. Y. Wong, K. G. Neoh, J. H. Song, J. W. P. Fu, S. Mhaisalkar, *et al.*, Critical parameters in the pegylation of gold nanoshells for biomedical applications: an in vitro macrophage study, *J. Drug Targeting*, 2009, **17**(3), 181–193.

21 P. Zhang, F. Sun, S. Liu and S. Jiang, Anti-PEG antibodies in the clinic: current issues and beyond PEGylation, *J. Controlled Release*, 2016, **244**, 184–193.

22 S. M. Fix, A. G. Nyankima, M. D. McSweeney, J. K. Tsuruta, S. K. Lai and P. A. Dayton, Accelerated clearance of ultrasound contrast agents containing polyethylene glycol is associated with the generation of anti-polyethylene glycol antibodies, *Ultrasound Med. Biol.*, 2018, **44**(6), 1266–1280.

23 T. Ishida, K. Atobe, X. Wang and H. Kiwada, Accelerated blood clearance of PEGylated liposomes upon repeated injections: effect of doxorubicin-encapsulation and high-dose first injection, *J. Controlled Release*, 2006, **115**(3), 251–258.

24 Y. Mima, Y. Hashimoto, T. Shimizu, H. Kiwada and T. Ishida, Anti-PEG IgM is a major contributor to the accelerated blood clearance of polyethylene glycol-conjugated protein, *Mol. Pharm.*, 2015, **12**(7), 2429–2435.

25 K. Yang, S. Zhang, G. Zhang, X. Sun, S.-T. Lee and Z. Liu, Graphene in mice: ultrahigh in vivo tumor uptake and efficient photothermal therapy, *Nano Lett.*, 2010, **10**(9), 3318–3323.

26 Y. Jin, J. Wang, H. Ke, S. Wang and Z. Dai, Graphene oxide modified PLA microcapsules containing gold nanoparticles for ultrasonic/CT bimodal imaging guided photothermal tumor therapy, *Biomaterials*, 2013, **34**(20), 4794–4802.

27 J. H. Lim, E.-J. Kim, C. D. Ahrberg and B. G. Chung, Functional graphene oxide-based nanosheets for photothermal therapy, *Macromol. Res.*, 2018, **26**(6), 557–565.

28 J. T. Robinson, S. M. Tabakman, Y. Liang, H. Wang, H. Sanchez Casalongue, D. Vinh, *et al.*, Ultrasmall reduced graphene oxide with high near-infrared absorbance for photothermal therapy, *J. Am. Chem. Soc.*, 2011, **133**(17), 6825–6831.

29 R. Lima-Sousa, D. de Melo-Diogo, C. G. Alves, E. C. Costa, P. Ferreira, R. O. Louro, *et al.*, Hyaluronic acid functionalized green reduced graphene oxide for targeted cancer photothermal therapy, *Carbohydr. Polym.*, 2018, **200**, 93–99.

30 Y. Wang, H. Wang, D. Liu, S. Song, X. Wang and H. Zhang, Graphene oxide covalently grafted upconversion nanoparticles for combined NIR mediated imaging and photothermal/photodynamic cancer therapy, *Biomaterials*, 2013, **34**(31), 7715–7724.

31 L. Yang, Y.-T. Tseng, G. Suo, L. Chen, J. Yu, W.-J. Chiu, *et al.*, Photothermal therapeutic response of cancer cells to aptamer–gold nanoparticle-hybridized graphene oxide under NIR illumination, *ACS Appl. Mater. Interfaces*, 2015, **7**(9), 5097–5106.

32 M. S. Khan, S. Pandey, M. L. Bhaisare, G. Gedda, A. Talib and H.-F. Wu, Graphene oxide@ gold nanorods for chemo-photothermal treatment and controlled release of doxorubicin in mice Tumor, *Colloids Surf., B*, 2017, **160**, 543–552.

33 J. Bai, Y. Liu and X. Jiang, Multifunctional PEG-GO/CuS nanocomposites for near-infrared chemo-photothermal therapy, *Biomaterials*, 2014, **35**(22), 5805–5813.

34 S. Chen, L. Li, C. Zhao and J. Zheng, Surface hydration: principles and applications toward low-fouling/nonfouling biomaterials, *Polymer*, 2010, **51**(23), 5283–5293.

35 J. Wu, W. Lin, Z. Wang, S. Chen and Y. Chang, Investigation of the hydration of nonfouling material poly (sulfobetaine methacrylate) by low-field nuclear magnetic resonance, *Langmuir*, 2012, **28**(19), 7436–7441.

36 Y. Men, S. Peng, P. Yang, Q. Jiang, Y. Zhang, B. Shen, *et al.*, Biodegradable zwitterionic nanogels with long circulation for antitumor drug delivery, *ACS Appl. Mater. Interfaces*, 2018, **10**(28), 23509–23521.

37 C. G. Alves, D. de Melo-Diogo, R. Lima-Sousa, E. C. Costa and I. J. Correia, Hyaluronic acid functionalized nanoparticles loaded with IR780 and DOX for cancer chemo-photothermal therapy, *Eur. J. Pharm. Biopharm.*, 2019, **137**, 86–94.

38 C. G. Alves, R. Lima-Sousa, D. de Melo-Diogo, R. O. Louro and I. J. Correia, IR780 based nanomaterials for cancer imaging and photothermal, photodynamic and combinatorial therapies, *Int. J. Pharm.*, 2018, **542**(1–2), 164–175.

39 C. Pais-Silva, D. de Melo-Diogo and I. J. Correia, IR780-loaded TPGS-TOS micelles for breast cancer photodynamic therapy, *Eur. J. Pharm. Biopharm.*, 2017, **113**, 108–117.

40 A. Venault, H.-S. Yang, Y.-C. Chiang, B.-S. Lee, R.-C. Ruaan and Y. Chang, Bacterial resistance control on mineral surfaces of hydroxyapatite and human teeth via surface charge-driven antifouling coatings, *ACS Appl. Mater. Interfaces*, 2014, **6**(5), 3201–3210.

41 J. C. Boga, S. P. Miguel, D. de Melo-Diogo, A. G. Mendonça, R. O. Louro and I. J. Correia, In vitro characterization of 3D printed scaffolds aimed at bone tissue regeneration, *Colloids Surf., B*, 2018, **165**, 207–218.

42 D. C. Marcano, D. V. Kosynkin, J. M. Berlin, A. Sinitskii, Z. Sun, A. Slesarev, *et al.*, Improved synthesis of graphene oxide, *ACS Nano*, 2010, **4**(8), 4806–4814.

43 C. Jiang, H. Cheng, A. Yuan, X. Tang, J. Wu and Y. Hu, Hydrophobic IR780 encapsulated in biodegradable human serum albumin nanoparticles for photothermal and photodynamic therapy, *Acta Biomater.*, 2015, **14**, 61–69.

44 M. J. Ernsting, M. Murakami, A. Roy and S.-D. Li, Factors controlling the pharmacokinetics, biodistribution and

Open Access Article. Published on 20 October 2020. Downloaded on 12/4/2025 10:06:17 PM.
This article is licensed under a Creative Commons Attribution-NonCommercial 3.0 Unported Licence.

intratumoral penetration of nanoparticles, *J. Controlled Release*, 2013, **172**(3), 782–794.

45 S.-D. Li and L. Huang, Pharmacokinetics and biodistribution of nanoparticles, *Mol. Pharm.*, 2008, **5**(4), 496–504.

46 Z. Dong, J. Mao, M. Yang, D. Wang, S. Bo and X. Ji, Phase behavior of poly (sulfobetaine methacrylate)-grafted silica nanoparticles and their stability in protein solutions, *Langmuir*, 2011, **27**(24), 15282–15291.

47 K. F. Chu and D. E. Dupuy, Thermal ablation of tumours: biological mechanisms and advances in therapy, *Nat. Rev. Cancer*, 2014, **14**, 199–208.

48 W. Ma, Y. Hu, H. Yang, Y. Zhang, J. Ding and L. Chen, Au-aided reduced graphene oxide-based nanohybrids for photo-chemotherapy, *Mater. Sci. Eng. C*, 2019, **95**, 256–263.

49 F. M. Kievit, O. Veiseh, N. Bhattarai, C. Fang, J. W. Gunn, D. Lee, *et al.*, PEI–PEG–chitosan-copolymer-coated iron oxide nanoparticles for safe gene delivery: synthesis, complexation, and transfection, *Adv. Funct. Mater.*, 2009, **19**(14), 2244–2251.

50 S. Zhang, C. Kucharski, M. R. Doschak, W. Sebald and H. Uludağ, Polyethylenimine–PEG coated albumin nanoparticles for BMP-2 delivery, *Biomaterials*, 2010, **31**(5), 952–963.

51 S. Nimesh, A. Aggarwal, P. Kumar, Y. Singh, K. Gupta and R. Chandra, Influence of acyl chain length on transfection mediated by acylated PEI nanoparticles, *Int. J. Pharm.*, 2007, **337**(1–2), 265–274.

52 S. Peng, B. Ouyang, Y. Men, Y. Du, Y. Cao, R. Xie, *et al.*, Biodegradable zwitterionic polymer membrane coating endowing nanoparticles with ultra-long circulation and enhanced tumor photothermal therapy, *Biomaterials*, 2020, **231**, 119680.

53 A. G. Almutary, B. J. Sanderson, Z. Alhalili and A. V. Ellis, Toxicity of thiolated silica nanoparticles modified with sulfobetaine methacrylate for potential use in chemotherapy drug conjugation, *J. Appl. Pharmaceut. Sci.*, 2017, **7**(07), 001–009.

54 J. Li, H. Hu, Z. Jiang, S. Chen, Y. Pan, Q. Guo, *et al.*, Near-infrared-induced IR780-loaded PLGA nanoparticles for photothermal therapy to treat breast cancer metastasis in bones, *RSC Adv.*, 2019, **9**(62), 35976–35983.

55 L. Xu, J. Wang, S.-Y. Lu, X. Wang, Y. Cao, M. Wang, *et al.*, Construction of a polypyrrole-based multifunctional nanocomposite for dual-modal imaging and enhanced synergistic phototherapy against cancer cells, *Langmuir*, 2019, **35**(28), 9246–9254.

 This journal is © The Royal Society of Chemistry 2020